The effect of karst system occurrence on flood peaks in small watersheds, southwest China

Chongxun Mo, Yafang Wang, Yuli Ruan, Junkai Qin, Mingshan Zhang, Guikai Sun and JuLiang Jin

ABSTRACT

Flooding at small basins is characterized by weak predictability, sudden onset, and rapid disaster formation, especially in karst areas. Therefore, an accurate flood simulation will be helpful for flood control and disaster reduction. In this study, the reservoir unit is added into the original HEC-HMS model to improve the model and analyze the stagnation of the runoff process in karst basins. Then, the HEC-HMS model before and after improvement is used to simulate floods in the Xiajia basin, a typical karst area in southwest China. Before improvement, the calibration result shows that the accuracy of 31 flood simulations is poor, and the qualified rate is only 38.71%. After improvement, the qualified rate increases to 51.61% during calibration, and the simulation accuracy is increased by 12.90%. Moreover, the qualified rate reaches 61.11% during validation, and the simulation accuracy is increased by 22.40%. The improved HEC-HMS model can be applied to flood simulations in the study area and the study results can provide useful insights for flood warning and management in karst areas.

Key words | flood simulation, HEC-HMS model, karst area, reservoir unit method, small basin

HIGHLIGHTS

- The novelty of this study lies in adding karst reservoir units to the HEC-HMS model to quantify the effect of the karst system on the surface flow in the Xiajia watershed, a typical karst area in southwest China.
- In this study, the results imply that the karst systems have an impact on the hydrology by effectively restraining the flood peak and increasing the underground runoff.

Chongxun Mo
Yafang Wang
Yuli Ruan (corresponding author)
Junkai Qin
Mingshan Zhang
Guikai Sun
College of Architecture and Civil Engineering,
Guangxi University,
Nanning,
China
E-mail: *mo_209@163.com*

Chongxun Mo
Yafang Wang
Yuli Ruan
Junkai Qin
Mingshan Zhang
Guikai Sun
Key Laboratory of Disaster Prevention and Structural Safety of Ministry of Education,
Nanning,
China

Chongxun Mo
Yafang Wang
Yuli Ruan
Junkai Qin
Mingshan Zhang
Guikai Sun
Guangxi Key Laboratories of Disaster Prevention and Engineering Safety,
Nanning,
China

JuLiang Jin
School of Civil Engineering,
Hefei University of Technology,
Hefei 230009,
China

INTRODUCTION

The increasing magnitude and frequency of flood disasters result in an increasing number of' human deaths and economic losses. Accurate flood simulation has been a hot topic in hydrological sciences as it is very helpful for flood warning, flood control, and flood disaster reduction. Commonly used hydrological models are often divided into two categories: the lumped hydrological model and the distributed hydrological model. The lumped hydrological model uses an approximate method to describe the runoff process without considering the physical mechanism of the hydrological phenomenon (Pan 2018). Therefore, distributed hydrological models with clear physical meaning parameters and accurate descriptions of the hydrological

doi: 10.2166/nh.2020.061

process have been developed and are widely used in hydrology (Gumindoga *et al.* 2017; Wang 2018a; Busico *et al.* 2020; Ferguson & Fenner 2020; Khaleghi *et al.* 2020). It is well known that karst fissures, sinkholes, and skylights are widely distributed in the karst basin, constituting a unique three-dimensional spatial system and making the hydrological process more complex. However, certain approaches for flood simulation in the karst basin remain limited. To improve the accuracy of flood simulation in the karst basin, researchers usually modify the original lumped or distributed hydrological model, as summarized in Table 1. As can be seen from Table 1, the improved hydrological models are only suitable for specific basins and have no universality. In addition, previous studies have shown that the HEC-HMS model has good accuracy for flood simulation in a small watershed (Kamali *et al.* 2013; Silva *et al.* 2014). In China, some studies have indicated that the HEC-HMS model is the optimum model for flood simulation in a small basin (Zhao *et al.* 2018; Zhang *et al.* 2019).

For southwest China, floods are the main disaster during the flood season. However, most of the basins are karst basins, with complex topography and geological conditions (Pu 2009). Karst peak clusters, sinkholes, and skylights are widely distributed, forming a unique three-dimensional spatial system. Thus, the mechanism of flood formation is more complex, and the simulations of the flooding are more difficult than those in non-karst basins. Therefore, the objective of this study is to add a karst reservoir unit to the HEC-HMS model to form a flood simulation tool for a small karst basin, the Xiajia basin in southwest China. Furthermore, this study tries to determine whether the added karst reservoir unit has a certain effect on the HEC-HMS model performance. The findings of this study can provide a useful insight for flood warning and management in karst areas.

STUDY AREA

The Xiajia basin is located in Lingyun County, Baise city, Guangxi, China, with a total catchment area of 799.20 km^2 and an average annual rainfall of 1,708.3 mm. Information for each station is shown in Table 2, and the location of the Xiajia basin is shown in Figure 1. There is a natural karst cave – water source cave – located on the southeast side of Lingyun County, and most of the runoff in the upper reaches of the cave is the underground undercurrent. The middle part of the Xiajia basin is hilly landform, while the northeast side has a karst peak-cluster depression topography. The basin is a typical karst basin in southwest China (Huang 1995).

HEC-HMS MODEL

Model construction

First, the DEM data with a resolution of 30 m was downloaded from www.gscloud.cn/. Then, HEC-GeoHMS was applied to obtain the sub-basins and river channel of the Xiajia basin, as shown in Figure 2 and Table 3. W01–W12 represent 12 sub-basin units, and R01–R05 represent four river channel units. In addition, soil data and land cover data with resolutions of 1×1 km were downloaded from the HWSD and IGBP_LUCC database, respectively, and the land cover and soil type of the Xiajia basin were obtained (Figure 3). The common methods for runoff calculation are the SCS curve method (Fang *et al.* 2007) and the initial losses-lateral losses method (Zhang *et al.* 2017). In this study, it was found that the SCS curve method had better results in the sub-basins W02–W04 and W06–W12, while the initial losses-lateral losses method had better results only in the sub-basins W01, W03 and W05. Therefore, the SCS curve method was adopted. As suggested by Ge (2016) and Wang (2018b), the Snyder unit line method was used for direct runoff confluence calculation, and the exponential attenuation method was applied to the base-flow separation. Finally, the Muskingum method was employed to calculate the river confluence due to its better applicability, fewer parameters, and easy calibration (Li 2020). The principle flow of the model is shown in Figure 4 (Li & He 2015).

SCS curve method

The calculation formulas of the SCS curve method are as follows (Bosznay 1989):

$$\frac{F}{S} = \frac{Q}{P - I_a} \tag{1}$$

$$I_a = 0.2S \tag{2}$$

$$CN = \frac{25400}{S + 254} \tag{3}$$

Table 1 | A summary of the application of the hydrological models in the karst basin

Classification	Name	Author	Improvements	Advantages and disadvantages
Lumped hydrological model	Xin'anjiang	Song *et al.* (2015b)	Added multiple series and parallel underground reservoirs for groundwater simulation	Advantages: Less data demand and a simple structure. Disadvantages: the physical meaning of parameters is not clear and it ignores the spatial variability of the basin and cannot explain the physical mechanism of runoff yield and concentration well
	Tank	Fleury *et al.* (2007)	Used three interconnected water tanks to simulate the flow in the soil and the underground runoff with different velocity	
Distributed hydrological model	SWAT	Palanisamy & Workman (2014)	Conceptualized the sinkholes located in the streambed of a karst watershed in Kentucky as orifices and flow through these orifices was modeled as a function of sinkhole diameter and added to the SWAT model to form a karst SWAT	Advantages: easy acquisition of input data and high calculation efficiency. Disadvantages: difficult to be used for short-term flood process simulation
		Baffaut & Benson (2009)	The SWAT model simulates lost streams by specifying high soil conductivity in channels, simulates sinkholes as ponds with high hydraulic conductivity at the bottom, and calibrates the James river watershed in southwestern Missouri	
		Nikolaidis *et al.* (2013)	The major modifications from the SWAT model are: (a) the input flow in the deep groundwater flow from SWAT and (b) a nitrate-N mass balance was included assuming that nitrate is conservative in the karst.	
	TOPMODEL	Suo *et al.* (2007)	Using the TOPMODEL model to calculate runoff yield in subwatershed	Advantage: it requires fewer parameters and is easy to obtain. Disadvantage: the description of the groundwater hydrological process is too simple, and DEM cannot be used to generate sinks and underground rivers in karst watershed
		Pan (2014)	Regard karst depression as an independent hydrological unit, and use the TOPMODEL model to simulate hydrology, respectively	
	SWMM	Campbell & Sullivan (2002)	The SWMM is used to simulate the transport process of karst cave water flow	Advantage: it can reflect the movement process of a flood wave in the pipeline more truthfully. Disadvantage: The SWMM is sensitive to the geometric characteristics of the pipeline and is only suitable for hydrological simulation of some pipeline systems with detailed survey data
		Zhang *et al.* (2007)	Taking the depression as a unit, the study area is generalized into six secondary catchment basins connected by pipeline	
	HEC-HMS	Current study	The reservoir unit method is used to reflect the stagnation of the runoff process in karst basins	The HEC-HMS model has good accuracy and is widely used at small basin

Table 2 | Discharge station information

Code	Name	Longitude	Latitude
20000900	Chaoli	106°30′14.736″E	24°14′21.567″N
20001300	Donghe	106°43′25.983″E	24°21′37.121″N
20000800	Lingyun	106°34′26.216″E	24°20′42.088″N
20001000	Xiajia	106°38′51.175″E	24°17′18.718″N

where CN is the empirical coefficient and can be determined depending on the land cover type and the soil hydrology group information, as shown in Table 4 (US Army Corps of Engineers 1994; Li & He 2015); I_a is the initial loss value of rainfall, mm; F is the total rainfall loss in the later period, mm; is the maximum retention in the basin, mm; Q is the flow, m^3/s; and P is the total precipitation, mm.S

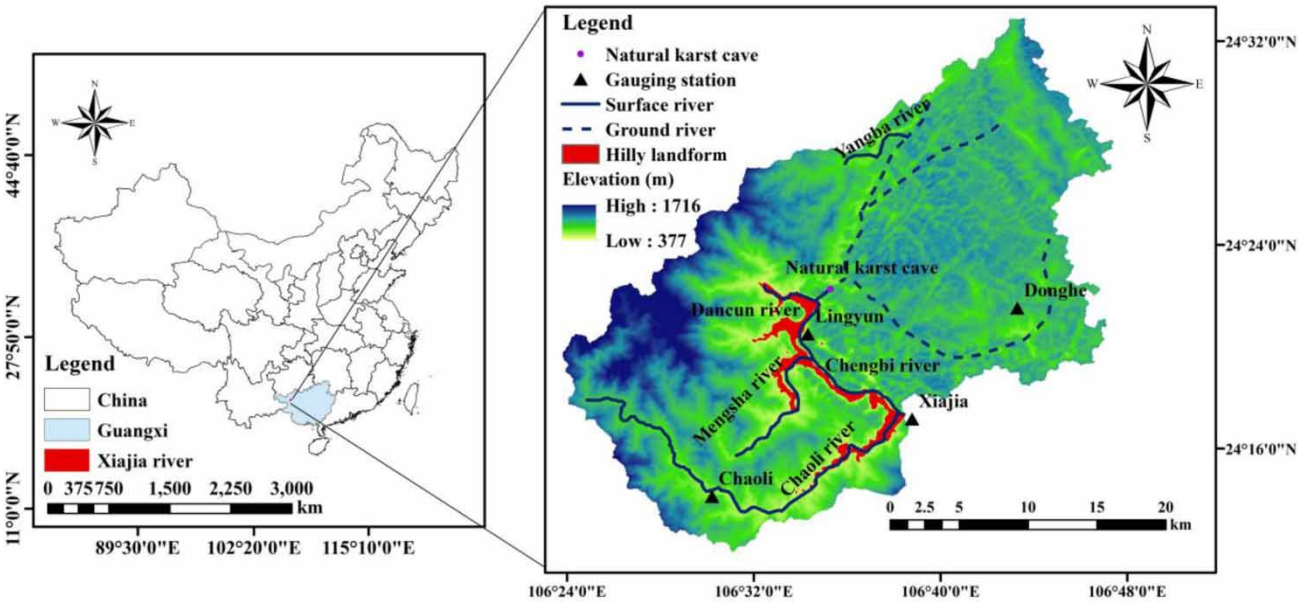

Figure 1 | The location of the Xiajia basin.

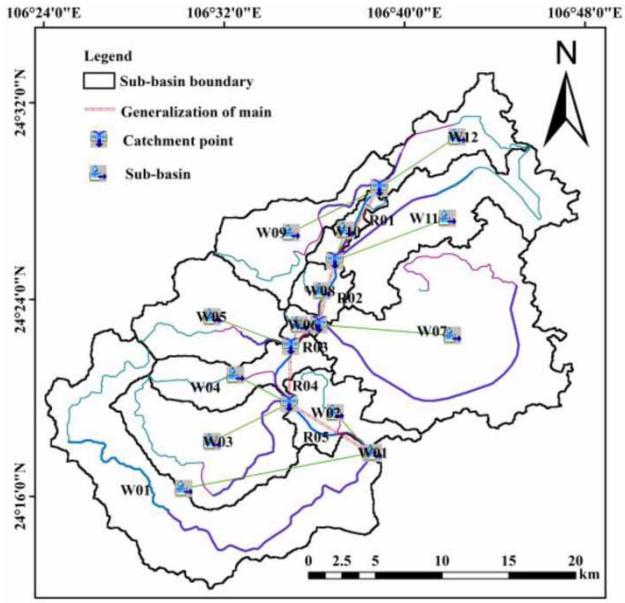

Figure 2 | Results of sub-basin division.

Table 3 | Basic information for sub-basins

Sub-basins	Area (km²)	Average slope (%)	Channel length (km)
W01	174.85	20.5	34.47
W02	34.94	32.5	8.06
W03	82.89	20.2	12.05
W04	38.90	24.1	5.47
W05	62.61	22.0	4.56
W06	5.60	25.1	2.79
W07	186.39	22.4	24.90
W08	14.92	25.9	5.41
W09	53.12	18.7	6.17
W10	11.25	24.2	6.84
W11	92.41	23.7	13.08
W12	41.34	21.3	3.24

Snyder unit line method

When using the Snyder unit line method, the time lag parameter t_p needs to be determined and can be calculated by the following empirical formula (Feng 2016):

$$t_p = \frac{\left(L^{0.8} \times \left(\left(\frac{1000}{CN} - 10\right) + 1\right)^{0.7}\right)}{1900 \times Y^{0.5}} \quad (4)$$

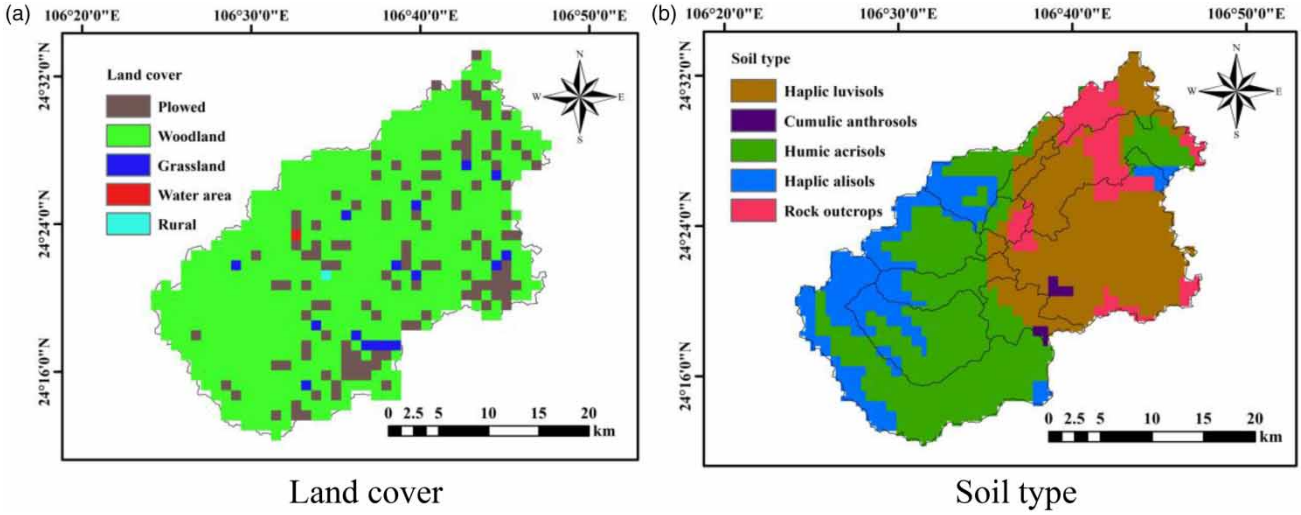

Figure 3 | Land cover and soil type.

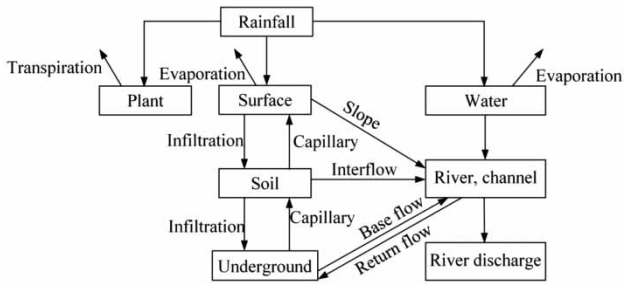

Figure 4 | Principle of the HEC-HMS model.

Table 4 | Summary of the land cover type and soil hydrology group

Land cover type	Hydrologic condition	Soil hydrology group			
		A	B	C	D
Cultivated land	Poor	76	85	90	93
	Good	74	83	88	90
Orchard grove	Poor	57	73	82	86
	Average	43	65	76	82
	Good	32	58	72	79
Woodland	Poor	48	68	77	83
	Average	35	56	70	77
	Good	30	48	65	73
Grasslands	/	30	58	71	78
Urban land	/	98	98	98	98

where L is the main river length; Y is the basin slope, %; and CN is the empirical coefficient of the SCS curve.

Exponential attenuation method

The exponential attenuation method is as follows (Cheng 2019):

$$Q_t = Q_0 k^t \tag{5}$$

where Q_0 is the initial base-flow, m^3/s; k is the attenuation coefficient that needs to be calibrated; and t is the time, h.

Muskingum method

The calculation formula of the Muskingum method is given as follows (Wang *et al.* 2018):

$$Q_{\text{down,end}} = C_0 Q_{\text{up,end}} + C_1 Q_{\text{up,start}} + C_2 Q_{\text{down,start}} \tag{6}$$

$$C_0 = \frac{0.5\Delta t - Kx}{K - Kx + 0.5\Delta t} \tag{7}$$

$$C_1 = \frac{0.5\Delta t + Kx}{K - Kx + 0.5\Delta t} \tag{8}$$

$$C_2 = \frac{K - Kx - 0.5\Delta t}{K - Kx + 0.5\Delta t} \tag{9}$$

where $Q_{\text{up,start}}$ and $Q_{\text{down,start}}$ are the upstream inflow and downstream inflow at the beginning of the period, respectively; $Q_{\text{up,end}}$ and $Q_{\text{down,end}}$ represent the upstream

outflow and downstream outflow at the end of the period, respectively; C_0, C_1 and C_2 are functions of K and x, respectively; $C_0 + C_1 + C_2 = 1$; K is the propagation time of steady flow in the reach, h; and x is the flow specific gravity coefficient.

Improved HEC-HMS model

A sub-basin is divided into karst areas and non-karst areas, and for karst areas, the karst features (natural karst cave, etc.) are considered as karst reservoirs, and the structure is shown in Figure 5. Suppose there is a sub-basin W_a, the sub-basin adjacent to W_a is W_b, and the direction of water flow is from W_a to W_b. Then, the flow yield in the karst area of W_a can be estimated by the karst reservoir (VB_1), and the water flowing from W_a to W_b is calculated by using a linear reservoir (VB_2) and the unit line method. The principle of the improved HEC-HMS model (Cheng 1988) is shown in Figure 6, and the constructions for karst reservoirs and linear reservoirs are as follows.

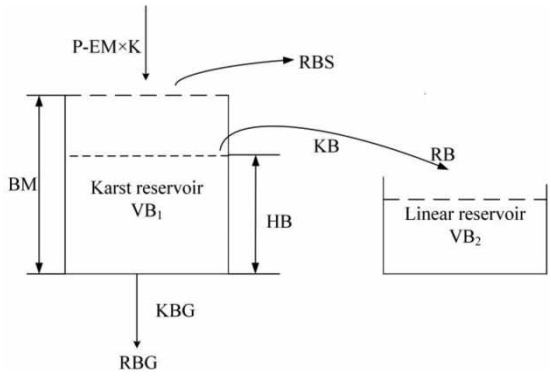

Figure 5 | Karst water storage structure.

Construction of karst reservoir (VB_1)

Surface runoff calculation. The surface runoff in the karst area of W_a is denoted as RBS and can be calculated as:

$$SB_t = SB_{t-1} + P_t - EM_t \times K \tag{10}$$

$$RBS_t = SB_t - BM, \ (SB_t > BM) \tag{11}$$

$$RBS_t = 0, (SB_t \leq BM) \tag{12}$$

where SB is the storage of the karst reservoir; P is the precipitation; EM is the evapotranspiration capacity; K is the

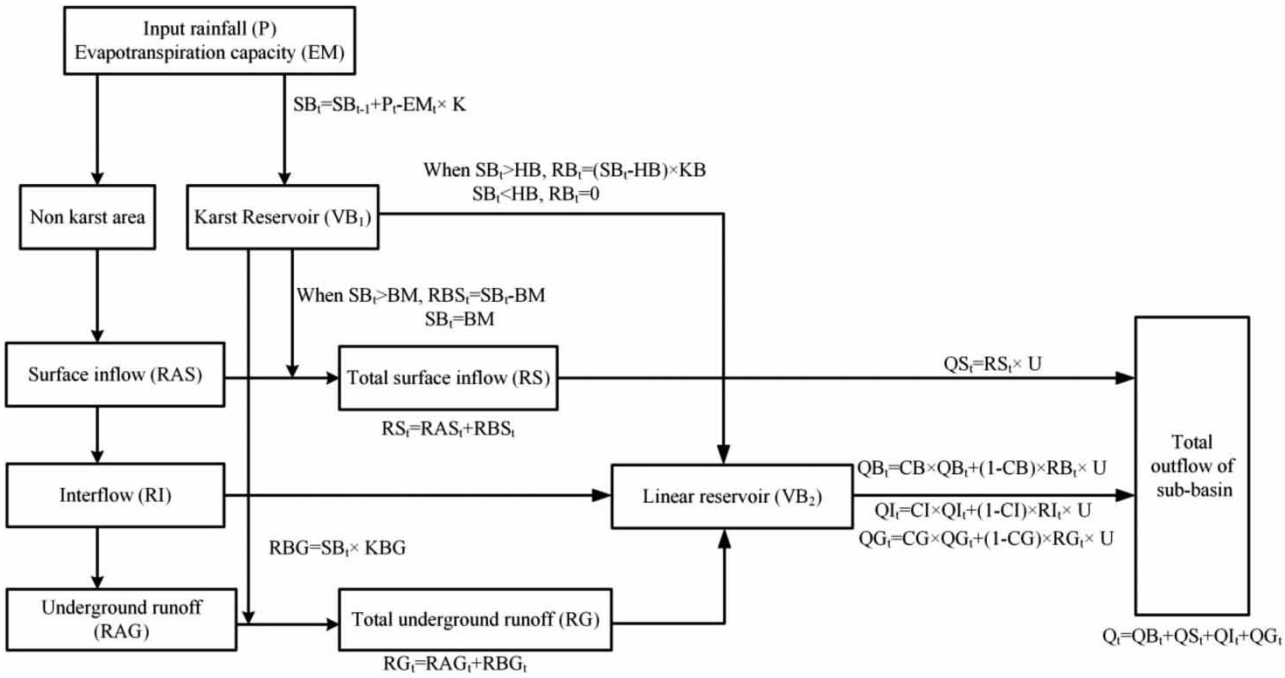

Figure 6 | Principle of the improved HEC-HMS model.

evaporation coefficient; BM is the maximum storage capacity of the karst reservoir; RBS is the surface runoff in the karst area of W_a.

Therefore, the total surface runoff in W_a can be calculated as:

$$RS_t = RBS_t + RAS_t \tag{13}$$

where RS is the total surface runoff in W_a and RAS is the surface runoff in the non-karst areas of W_a.

Karst conduit flow. The karst conduit flow in the karst area of W_a is denoted as RB and can be calculated as:

$$RB_t = (SB_t - HB) \times KB \tag{14}$$

where RB is the karst conduit flow; HB is the threshold value; and KB is the outflow coefficient of karst conduit flow.

Underground runoff. The underground runoff in the karst area of W_a is denoted as RBG and can be calculated as:

$$RBG = SB_t \times KBG \tag{15}$$

where RBG is the underground runoff in the karst area of W_a and KBG is the linear outflow coefficient.

Therefore, the total underground runoff in W_a can be calculated as:

$$RG_t = RBG_t + RAG_t \tag{16}$$

where RG is the total underground runoff of W_a and RAG is the underground runoff in the non-karst areas of W_a.

Construction of linear reservoirs (VB_2)

Interflow. The interflow (QI) flowing from the non-karst areas of W_a to W_b can be calculated as:

$$QI_t = CI \times QI_{t-1} + (1 - CI) \times RI_t \times u \tag{17}$$

where CI is the regression coefficient of the soil mid-stream reservoir; RI is the interflow; and u is the unit conversion coefficient.

Karst conduit flow. The karst conduit flow flowing from the karst areas of W_a to W_b can be denoted as QB and calculated as:

$$QB_t = CB \times QB_{t-1} + (1 - CB) \times RB_t \times u \tag{18}$$

where CB is the regression coefficient of the karst water and u is the unit conversion coefficient.

Underground runoff. The underground runoff flowing from W_a to W_b is denoted as QG and can be calculated as:

$$QG_t = CG \times QG_{t-1} + (1 - CG) \times RG_t \times u \tag{19}$$

where CG is the regression coefficient of the groundwater reservoir and u is the unit conversion coefficient.

RESULTS

Calibration result for the initial HEC-HMS model

The discharge and precipitation data (2002–2018) used in this study were recorded by Chaoli, Donghe, Lingyun and Xiajia stations and provided by the Chengbi River Reservoir Management Bureau. Wang *et al.* (2019) showed that the determination of hydrological model parameters is closely related to the flood peak and the flood volume of the flood used during the calibration. A calibration using variable size flood samples is helpful to obtain more stable and representative model parameters. Therefore, 31 different size flood samples were applied to calibrate the model in this study. Among the flood samples, the maximum flood peak was 358 m^3/s (number 20100628), the minimum flood peak was 101 m^3/s (number 20050614), the average value was 179 m^3/s, and the standard deviation was 69 m^3/s. Take the maximum measured flood peak (358 m^3/s) as the reference and take one-third (119 m^3/s) and two-thirds (239 m^3/s) as the bases for flood classification. Finally, the samples can be divided into three categories: category (i) ($Q_m < 119$ m^3/s), category (ii) (119 $m^3/s < Q_m < 239$ m^3/s), and category (iii) ($Q_m > 239$ m^3/s). The flood and their corresponding rainfall samples are shown in the appendix (Supplementary material, Table A1). In addition, to study the influence of

the rainfall data with different centers on the model simulation results, the watershed was divided into four different rainfall centers and the division results are shown in Figure 7 (Sun *et al.* 2014).

The relative error (Re) of the flood peak, the Re of the flood volume, the deviation of the peak time Δt, and the Nash efficiency coefficient (N_{SE}) (Moriasi *et al.* 2007) were selected as the evaluation indices of the model simulation accuracy. A simulation with $Re \leq 20\%$, $\Delta t \leq 3$ h, and $N_{SE} \geq 0.5$ can be considered as a qualified simulation. Additionally, the square of R (R^2) and the mean absolute error (MAE) were applied to give a better understanding of the overall goodness-of-fitness. The optimization parameters obtained by the Nelder–Mead method (Zettel & Hitzmann 2017) were substituted into the initial HEC-HMS model to simulate 31 floods in the calibration period, and the parameters are shown in the appendix (Supplementary material, Table A3). Finally, it is shown that the simulation result was poor, and the qualified rate ($n/N \times 100\%$, n is the number of qualified simulations, N is the number of total simulations) was only 38.71%. Due to space limitations, only the simulations with three different size flood samples numbered 20080926 (category i), 20050620 (category ii), and 20100628 (category iii) were analysed, and the results are shown in Table 5 and Figure 8. For the simulation with flood sample numbered 20080926, the simulated curve and measured curve were close, and the peak time was the same, but the simulated flood peak and flood volume were slightly larger than the measured values. After the flood peak, a small amount of precipitation also caused obvious fluctuation in the simulated flow. The Re values of the flood peak and flood volume were 23.53 and 40.65%; the was 0; and the N_{SE}, R^2, and MAE were 0.38, 0.96 and 18.9, respectively. For the simulation with the flood sample numbered 20050620, the simulated flood peak was obviously larger than the measured value, Δt and the simulated flood volume was slightly larger than the measured value. After the flood peak, there was also a fluctuation in the large flow caused by small precipitation. The Re values of the flood peak and flood volume were 76.09 and 10.14%, the Δt was –11, and the N_{SE}, R^2, and MAE were –1.5, 0.82 and 26.3. For the simulation with the flood sample numbered 20100628, the simulated flood peak and flood volume were far beyond the measured values. The Re values of the flood peak and flood volumes were 149.44 and 182.17%, the Δt was 4, and the N_{SE}, R^2, and MAE were –15.6, 0.69 and 284.2, respectively.

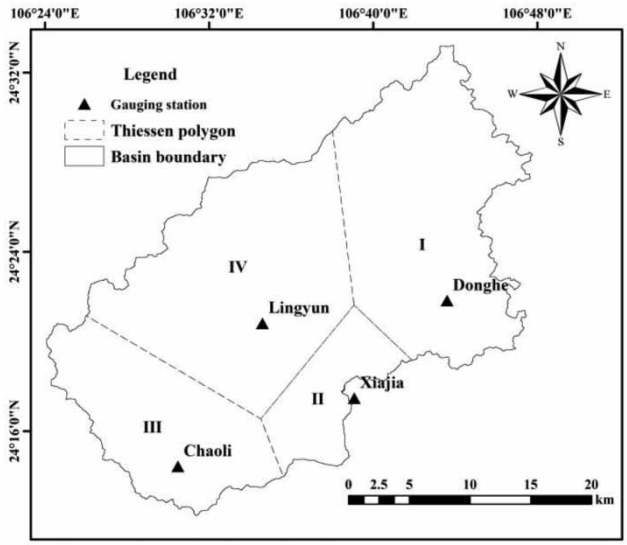

Figure 7 | Indication of precipitation gravity center zoning.

Flood simulation by using the improved HEC-HMS model

Calibration results

The precipitation and flood samples used in the calibration for the improved HEC-HMS model are the same as for the

Table 5 | Calibration results for the initial HEC-HMS model

	Flood peak (m^3/s)			Deviation of peak time (h)			Flood volume (mm)					
Flood number	Mea	Sim	Re (%)	Mea	Sim	Δt	Mea	Sim	Re (%)	N_{SE}	R^2	MAE
20080926	119	147	23.53	14:00	14:00	0	21.4	30.1	40.65	0.38	0.96	18.9
20050620	138	242.6	76.09	21:00	8:00	–11	66.1	72.8	10.14	–1.5	0.82	26.3
20100628	358	892.5	149.44	6:00	10:00	4	57.2	161.4	182.17	–15.6	0.69	284.2

Mea is measurement; Sim is simulation.

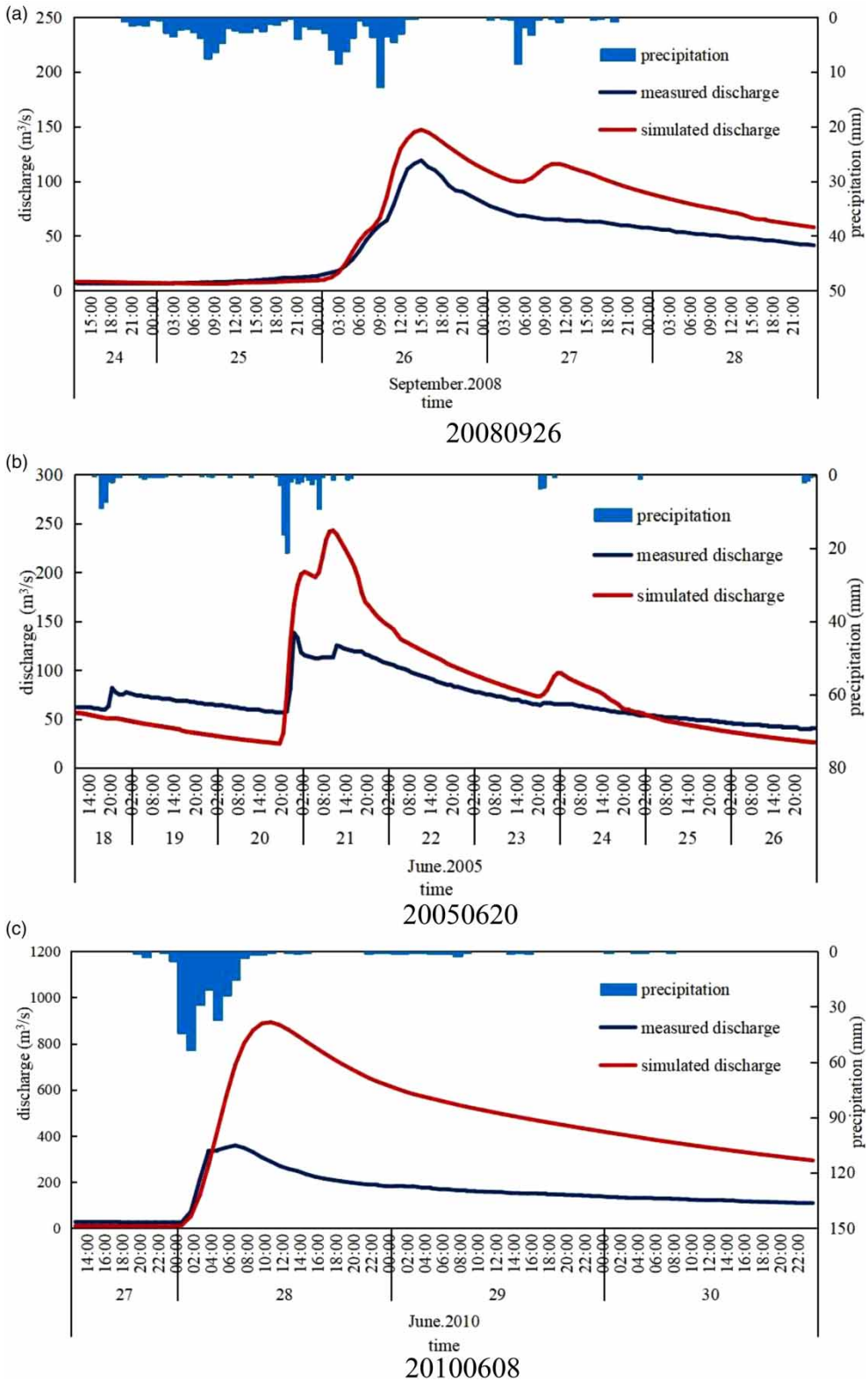

Figure 8 | Calibration results for the initial HEC-HMS model.

initial HEC-HMS model. The simulation results are summarized in Table 6. Overall, 16 of the 31 simulations are qualified, and the qualified rate is 51.61%. Among the unqualified simulations, six simulations are unqualified for the Re of the flood peak, seven simulations are unqualified for the Δt, eight simulations are unqualified for the Re of the flood volume, and seven simulations are unqualified for the Nash efficiency coefficient. In addition, the spatial variation of the evaluation indices is shown in Figure 9. Six precipitation centers fall in zone I, and the corresponding qualified rate of the flood simulation is 66.67%, the NSE value is 0.93, and R^2 is 0.94. Five precipitation centers fall in

Table 6 | Simulation results for the improved HEC-HMS model during calibration

	Peak (m^3/s)			Peak time (h)			Flood volume (mm)				
Flood number	**Mea**	**Sim**	**Re (%)**	**Mea**	**Sim**	**Δt**	**Mea**	**Sim**	**Re (%)**	**N_{SE}**	**Qualified**
20020602	125	119	4.80	7:00	6:00	1	38.0	36.6	3.68	0.95	Yes
20020616	126	150	19.05	8:00	5:00	3	41.4	38.3	7.49	0.48	No
20020630	138	114	17.39	10:00	11:00	–1	30.0	26.9	10.33	0.88	Yes
20020721	115	176	53.04	11:00	16:00	19	35.0	37.2	6.29	0.39	No
20030528	130	149	14.62	12:00	12:00	0	28.1	26.5	5.69	0.51	Yes
20030610	127	161	26.77	6:00	0:00	6	48.6	48.2	0.82	0.90	No
20030622	327	338	3.36	2:00	2:00	0	60.8	73.8	21.38	0.67	No
20030720	139	137	1.44	12:00	12:00	0	19.3	23.0	19.17	0.63	Yes
20030726	157	113	28.03	10:00	20:00	–12	64.8	46.2	28.70	0.42	No
20040626	102	55	46.08	9:00	20:00	–11	29.8	17.6	40.94	–2.57	No
20040710	251	238	5.18	21:00	22:00	–1	50.6	56.6	11.86	0.90	Yes
20040721	160	203	26.88	5:00	0:00	5	70.3	66.4	5.55	0.77	No
20050606	138	120	13.04	6:00	6:00	0	39.5	35.5	10.13	0.81	Yes
20050614	101	116	14.85	7:00	6:00	1	16.3	18.3	12.27	–0.22	No
20050620	138	161	16.67	21:00	6:00	–9	66.1	58.6	11.35	0.53	No
20060708	195	195	0.00	6:00	6:00	0	46.1	48.4	4.99	0.98	Yes
20060718	158	169	6.96	14:00	12:00	2	63.8	49.7	22.10	0.32	No
20060806	211	232	9.95	9:00	6:00	3	78.1	69.6	10.88	0.92	Yes
20070628	187	120	35.83	4:00	4:00	0	29.3	32.2	9.90	0.73	No
20070903	149	145	2.68	14:00	13:00	1	24.8	26.8	8.06	0.86	Yes
20070909	200	181	9.50	8:00	9:00	–1	49.1	48.2	1.83	0.98	Yes
20080530	139	149	7.19	8:00	9:00	–1	23.0	30.7	33.48	0.82	No
20080609	167	152	8.98	12:00	9:00	3	44.5	43.0	3.37	0.92	Yes
20080612	325	319	1.85	11:00	10:00	1	50.1	58.5	16.77	0.77	Yes
20080813	137	128	6.57	13:00	11:00	2	27.3	25.7	5.86	0.88	Yes
20080926	119	136	14.29	14:00	11:00	3	21.4	24.9	16.36	0.88	Yes
20081103	103	114	10.68	20:00	23:00	21	49.4	35.8	27.53	0.50	No
20100628	358	337	5.87	6:00	7:00	–1	57.2	69.1	20.80	0.69	No
20100721	222	263	18.47	10:00	10:00	0	86.1	94.5	9.76	0.73	Yes
20120521	273	322	17.95	6:00	6:00	0	46.9	67.2	43.28	–0.12	No
20120608	244	263	7.79	12:00	12:00	0	112.2	120.8	7.66	0.63	Yes

Mea is measurement; Sim is simulation.

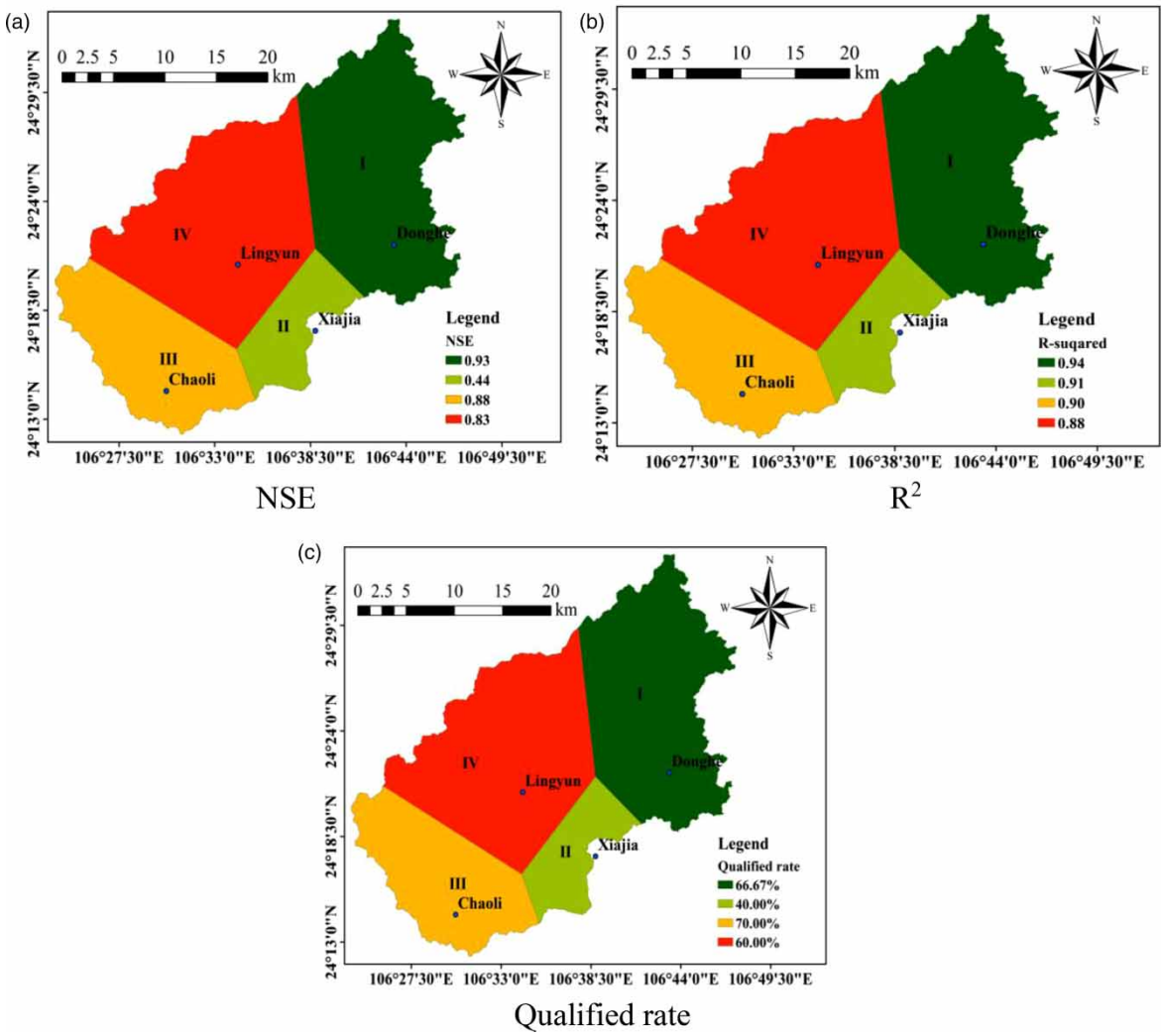

Figure 9 | The spatial variation of the evaluation indices in the calibration. (a) NSE; (b) R^2; and (c) Qualified rate.

zone II, and the corresponding qualified rate of the flood simulation is 40.00%, the NSE value is 0.44, and R^2 is 0.91. Ten precipitation centers fall in zone III, and the corresponding qualified rate of the flood simulation is 70.00%, the NSE value is 0.88, and the R^2 value is 0.90. Ten precipitation centers fall in zone IV, and the corresponding qualified rate of the flood simulation is 60.00%, the NSE value is 0.83, and R^2 is 0.88. Thus, the correlation between the flood simulation effectiveness and precipitation center is not significant, and the difference in the precipitation center has little effect on the flood simulation result. Additionally, according to precipitation forcing of the People's Republic of China (GB/T 28592–2012), 24-hour rainfall can be divided into six grades: light rain, moderate rain, heavy rain, rainstorms, heavy rainstorms, and extraordinary rainstorms. It was found that among the precipitation samples, one sample was heavy rain, and the corresponding flood simulation result was unqualified. Eight samples were rainstorms, and the maximum precipitation was 96.74 mm, the minimum precipitation was 54.18 mm, the average was 76.03 mm, the standard deviation was 12.62, and the corresponding flood simulation qualified rate was 87.5%. Twenty samples were heavy rainstorms, and the maximum and minimum precipitation were 239.46 and 102.71 mm, respectively. The average was 160.17 mm, the standard deviation was 41.38, and the

corresponding flood simulation qualified rate was 55.0%. Two samples were extraordinary rainstorms, and the maximum precipitation was 263.63 mm, the minimum precipitation was 253.18 mm, the average was 258.41 mm, the standard deviation was 7.39, and the corresponding flood simulation qualified rate was 50.0%. For flood peak type, 19 floods were single-peak, with concentrated corresponding precipitation processes and large flood peak values, and the qualified rate was 73.68%. Twelve floods were multi-peak, with relatively scattered corresponding precipitation processes, and the qualified rate was 41.67%. The flood simulation effectiveness was related to the flood peak type, and the flood simulation effectiveness of the single-peak floods was better than that of the multi-peak floods.

Based on the comprehensive analysis of the precipitation level, precipitation center and flood peak type, it can be concluded that the HEC-HMS model constructed in this study has better simulation results under the conditions of heavy rainfall and concentrated precipitation processes.

Validation results

The precipitation and flood samples used in the validation for the improved HEC-HMS model included 18 different size flood samples and their corresponding precipitations, and the simulation results are summarized in Table 7. Overall, 11 simulations were qualified, and the qualified rate was 61.11%. Three floods were selected as the representative, and the variation of flood hydrograph and karst storage is shown in Figure 10. It can be seen from Figure 10 that the karst storage was variable, which shows that the karst reservoir unit can simulate the stagnation of the runoff process in the karst area well. In addition, the spatial variation of the evaluation indices is shown in Figure 11. One precipitation center falls in zone I, and the corresponding qualified rate of the flood simulation was 100% with the NSE and R^2 values of 1.00. Two precipitation centers fall in zone II, and the corresponding qualified rate of the flood simulation was 100.00% with the NSE and R^2 values of 1.00. Seven precipitation centers fall in zone III, and the corresponding

Table 7 | Simulation results for the improved HEC-HMS model during validation

	Flood peak (m^3/s)			Peak time (h)			Flood volume (mm)				
Flood number	Mea	Sim	Re (%)	Mea	Sim	Δt	Mea	Sim	Re (%)	N_{SE}	Qualified
20141004	163	155.4	4.66	10:00	10:00	0	36.6	36.4	0.55	0.94	Yes
20150523	161	200.2	24.35	5:00	3:00	2	71.5	87.0	21.68	0.60	No
20150621	159	186.5	17.30	16:00	14:00	2	49.2	49.2	0.00	0.77	Yes
20150704	160	190.3	18.94	8:00	7:00	1	69.9	70.5	0.86	0.87	Yes
20150819	205	252.3	23.07	12:00	11:00	1	50.8	61.3	20.67	0.61	No
20150829	110	141.9	29.00	14:00	12:00	2	58.1	54.5	6.20	0.57	No
20170616	115	121.5	5.65	8:00	5:00	3	51.7	45.2	12.57	0.66	Yes
20170628	106	132.5	25.00	7:00	6:00	1	56.1	48.2	14.08	0.51	No
20170712	195	199	2.05	7:00	8:00	–1	61.5	49.0	20.33	0.83	No
20170809	144	155	7.64	8:00	6:00	2	47.9	39.9	16.70	0.56	Yes
20170814	222	262	18.02	7:00	17:00	–10	54.6	58.6	7.33	0.50	No
20170825	126	134	6.35	7:00	19:00	12	38.1	37.2	2.36	0.84	No
20170906	111	97	12.61	13:00	11:00	2	45.7	39.9	12.69	0.56	Yes
20180604	106	116	9.43	16:00	13:00	3	28.7	28.0	2.44	0.77	Yes
20180624	148	153	3.38	6:00	4:00	2	49.7	40.6	18.31	0.78	Yes
20180709	217	214	1.38	5:00	3:00	2	55.2	50.9	7.79	0.90	Yes
20180808	321	323	0.62	6:00	6:00	0	118.6	110.1	7.17	0.70	Yes
20180902	216	203	6.02	2:00	3:00	–1	27.3	31.0	13.55	0.90	Yes

Mea is measurement; Sim is simulation.

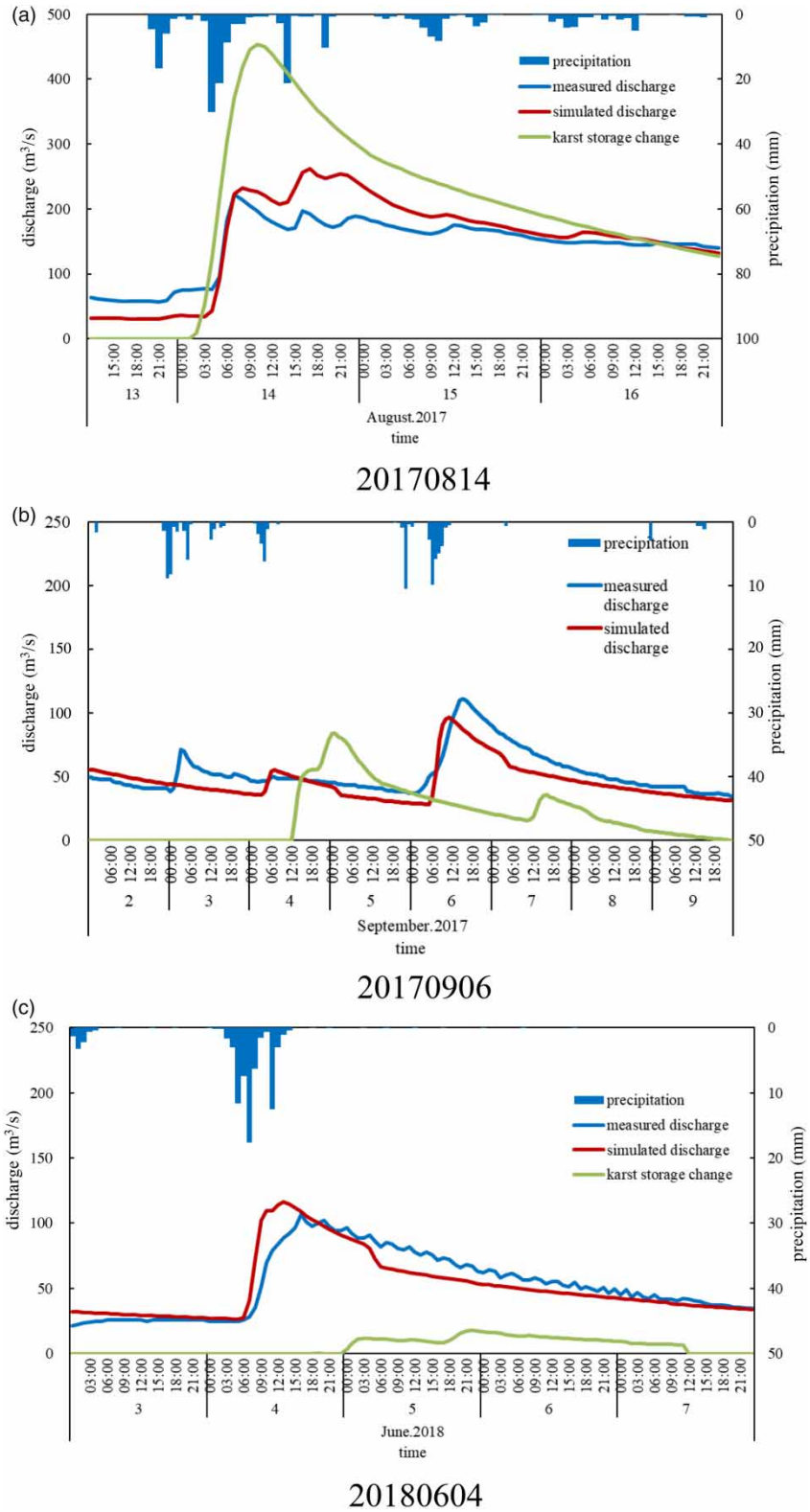

Figure 10 | Changes in flood hydrograph and karst storage. (a) 20170814, (b) 20170906, (c) 20180604.

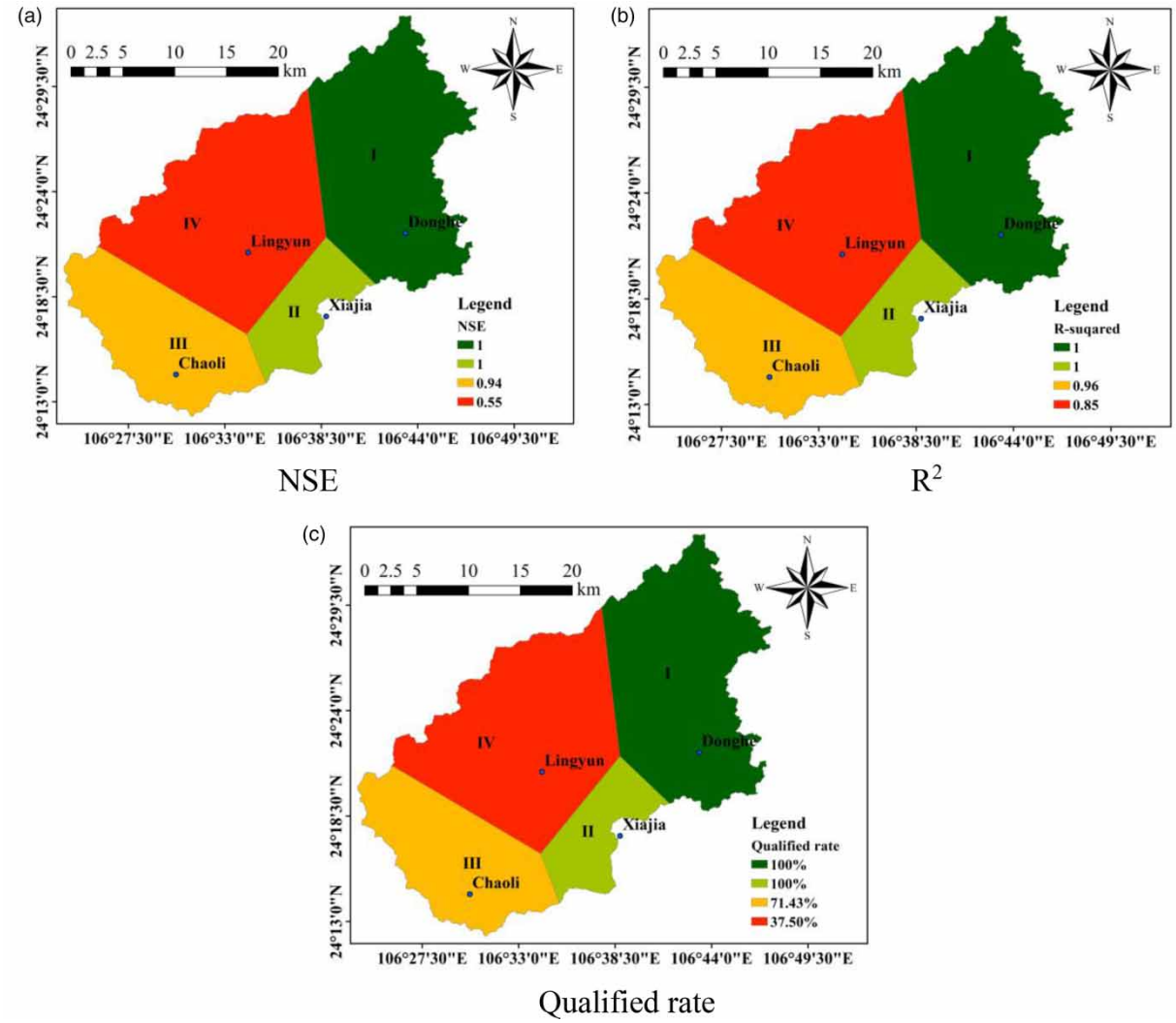

Figure 11 | The spatial variation of the evaluation indices in the validation. (a) NSE; (b) R^2; and (c) Qualified rate.

qualified rate of the flood simulation was 71.43% with the NSE value of 0.94 and R^2 of 0.96. Eight precipitation centers fall in zone IV, and the corresponding qualified rate of the flood simulation was 37.50% with the NSE value of 0.55, and R^2 of 0.85. For precipitation level, three precipitation samples were rainstorms, the maximum precipitation was 95.49 mm, the minimum precipitation was 76.63 mm, the average was 84.90 mm, the standard deviation was 10.00, and the simulation qualified rate was 66.67%. Thirteen precipitation samples were heavy rainstorms with the maximum and minimum values of 203.06 and 109.58 mm. The average was 141.45 mm, the standard deviation was 23.83, and the simulation qualified rate was 61.54%. Two precipitation samples were extraordinary rainstorms with maximum and minimum values of 301.38 and 273.51 mm, respectively. The standard deviation was 19.71, and the simulation qualified rate was 50.00%. For flood peak type, nine flood samples were single-peak with concentrated corresponding precipitation processes and large flood peak values, and the qualified rate was 77.78%. Nine flood samples were multi-peak with relatively scattered corresponding precipitation processes, and the qualified rate was 44.44%. The flood simulation effectiveness is related to the flood peak type, and the flood simulation effectiveness of the single-peak floods is better than that of the multi-peak floods.

DISCUSSION

The calibration results of the original HEC-HMS model are generally poor, and the simulated values overestimate the measured values. To determine the reasons why the simulation results are poor, three hypotheses are proposed: (1) there are incorrect parameter values; (2) the studied basin is not a closed basin due to the influence of karst landforms, leading to a large number of flows flowing down to other basins through karst pipelines (Xu *et al.* 2017); and (3) the karst cave, called a water source cave, has a detention effect on floods (Chen 2018).

For assumption (1), the Morse method (Song *et al.* 2015a) is applied to analyze the sensitivity $(e_i = y_i* - y/\Delta i)$ of the parameters, and the results are shown in Table 8 and Figure 12. Taking the floods numbered 20080926, 20050620, and 20100628 as examples, for flood peak, *CN* is the most sensitive parameter (*e* ranges from 5.818 to 13.451), followed by *Cp*, t_p and I_a. For peak time, the sensitivity of each parameter is low, among which, C_p is the most sensitive parameter (*e* ranges from 0.050 to 0.100), followed by *K* and t_p. For flood volume, *CN* is the most sensitive parameter (*e* ranges from 1.596 to 2.438), followed by C_p, t_p, *k* and *r*. The above sensitivity analysis results imply that adjusting the sensitive parameters can change the simulation output and therefore improve the simulation accuracy of the model to a certain extent. However, an over-adjustment of the model parameters may make it lose its actual physical meaning. For example, when the *CN* value in this study drops to approximately one-third of its initial value, the simulated flood peak value of the large flood is equivalent to the measured value, but the *CN* value will be far from that of the land condition represented by the original land cover and soil hydrological group. Chen *et al.* (2016) and Liao (2017) also proved that it is unreasonable to significantly reduce the *CN* value. Therefore, it is believed that the values of the parameters in this study are reasonable and that they are not the main cause of the low accuracy simulation.

For assumption (2), an analysis of water balance is applied to find out whether the studied basin is a closed basin or not, and the results are shown in Table 9. In terms of multi-year averages, the water of the studied basin is unbalanced, which implies that the studied basin is not a closed basin. However, the value of $R/P - E = 2.668 > 0$ implies that some water from the adjacent basin may flow into the studied basin through karst pipes. Thus, assumption (2) is not true.

For assumption (3), as stated above, a natural karst cave, called a water source cave, is located in sub-basin W06. The calibration results show that the simulated values with the flood samples that belong to category i are similar to the measured values, while the simulated values with the flood samples that belong to category iii are far beyond the measured values. This phenomenon can be explained from the perspective of detention storage, that is, when the incoming flow is small, it is the free outflow of the open channel, and as the discharge increases, it gradually changes to pressure orifice outflow, and therefore, some water cannot be discharged and stagnate in the karst area during the flooding time, and finally this water will gradually discharge after the flood recedes. This suggests that the

Table 8 | Calculations of the sensitivity of the parameters

	Flood peak			Peak time			Flood volume		
Parameter	**20080926**	**20050620**	**20100628**	**20080926**	**20050620**	**20100628**	**20080926**	**20050620**	**20100628**
CN	7.367	5.818	13.451	0.022	0.067	0.044	2.152	1.596	2.438
I_a	0.929	0.982	1.636	0.000	0.044	0.000	0.223	0.280	0.292
t_p	1.744	1.171	3.573	0.000	0.067	0.044	0.306	0.171	0.510
C_p	2.460	1.113	6.148	0.050	0.075	0.100	0.296	0.274	0.626
K	0.549	0.711	0.220	0.000	0.000	0.000	0.324	1.238	0.849
R	0.000	0.036	0.000	0.000	0.000	0.000	0.310	0.544	0.709
K	0.013	0.080	0.076	0.000	0.089	0.000	0.003	0.000	0.008
X	0.000	0.011	0.000	0.000	0.000	0.000	0.000	0.000	0.000

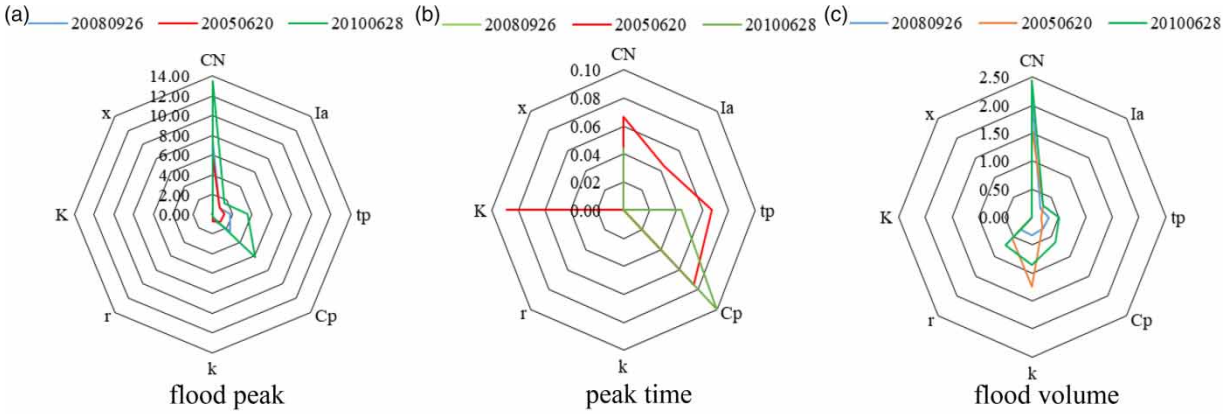

Figure 12 | Sensitivity comparison of each parameter: (a) flood peak; (b) peak time; and (c) flood volume.

Table 9 | Calculations of water balance for different watersheds

Annual average precipitation (P)/mm	Annual average evaporation (E)/mm	Annual average runoff (R)/mm	$\frac{R}{P-E}$
1,569.2	1,332.7	631	2.668

drainage basin in the karst area above the water source cave has a stagnant effect on water flow. Thus, assumption (3) is reasonable.

Additionally, it should be noted that although the simulation result has been improved after adding a reservoir unit to the original HEC-HEM model, the simulation accuracy of this study is still low compared to that in non-karst basins (Feng 2016). The reason may be that the hydrological processes in karst basins are extremely complex, and not all the karst features and their effects can be considered in the model improvement, resulting in some errors. In addition, it is found that the model will have better simulation results when the rainfall is heavy and the precipitation process is concentrated. The reason may lie in that when the rainfall runoff is heavy, the rapid flow increases. Meanwhile, the evaporation and the karst underground pipe network consumption are relatively small. Therefore, the simulation accuracy is relatively high.

CONCLUSIONS

An accurate flood simulation is crucial for flood warning, flood control, and flood disaster reduction, especially in karst areas with more complex flood features. Therefore, the objective of this study was to add a karst reservoir unit to the HEC-HMS model to analyze the impact of karst system occurrence on flood peaks and form a more accurate model for flood simulation. Some major findings were as follows: The HEC-HMS model with a karst reservoir unit outperformed the original model. After adding the karst reservoir unit, the qualified rate was increased by 22.40 and 22.58% during calibration and validation, respectively. Furthermore, for flood peaks and flood volumes, the parameter *CN* was the most sensitive parameter, followed by C_p and t_p. Also, a comprehensive analysis of the flood sample data (Tables A1 and A2 in the Supplementary material) and simulation results (Tables 6 and 7) showed that the results were better for the simulation with a rainstorm and a single-peak type flood than that with a non-rainstorm and a multi-peak type flood. Additionally, the simulation results were better when the gravity center of precipitation fell in zone III, zone I, and zone IV.

The novelty of this study lay in adding a karst reservoir unit to the HEC-HMS model to quantify the effect of the karst system on the surface flow in a karst basin. Finally, the results implied that karst systems had an impact on hydrology by effectively restraining flood peaks and increasing underground runoff, which agreed with the findings of Bailly-Comte *et al.* (2008), Palanisamy & Workman (2014), and Zhao *et al.* (2019). However, some shortcomings remain to be addressed. Only one hydrological station is located in the studied basin, meaning the model has to be calibrated and validated by the data from one hydrological

station. Further hydrological research is required to study the application of a reservoir unit in flood modelling at karst basins. Additionally, the differences in runoff parameters between karst areas and non-karst areas, the alternation of open flow and buried flow, and the mutual conversion between surface water and groundwater need to be further studied, and some useful advice can be found in Sun (2015). Besides, only one basin in Guangxi Province was considered in this study, and it is not realistic to extrapolate the findings of this study to larger spatial scales. Thus, more universal results need to be studied.

ACKNOWLEDGEMENTS

The authors are grateful for the support of the Natural Science Foundation of China (51969004 and 51579059), the National Key Research and Development Program of China (2017YFC1502405 and 2016YFC0401303), the Guangxi Natural Science Foundation of China (2017GXNSFAA198361), and the Innovation Project of Guangxi Graduate Education (YCBZ2019022).

DATA AVAILABILITY STATEMENT

All relevant data are included in the paper or its Supplementary Information.

REFERENCES

Baffaut, C. & Benson, V. W. 2009 Modeling flow and pollutant transport in a karst watershed with SWAT. *Transactions of the ASABE* **52** (2), 469–479.

Bailly-Comte, V., Jourde, H., Roesch, A., Pistre, S. & Batiot-Guilhe, C. 2008 Time series analyses for karst/river interactions assessment: case of the Coulazou river (southern France). *Journal of Hydrology* **349** (1–2), 98–114.

Bosznay, M. 1989 Generalization of SCS curve number method. *Journal of Irrigation & Drainage Engineering* **115** (1), 139–144.

Busico, G., Nicolo, C., Fronzi, D., Pellegrini, M. & Micol, M. 2020 Evaluating SWAT model performance, considering different soils data input, to quantify actual and future runoff susceptibility in a highly urbanized basin. *Journal of Environmental Management* **266**, 110625.

Campbell, C. W. & Sullivan, S. M. 2002 Simulating time-varying cave flow and water levels using the Storm Water Management Model. *Engineering Geology* **65** (2–3), 133–139.

Chen, S. 2018 *Research on Quantitative Evaluation Method of Groundwater Resources in Southwest Karst Peak Forest Area*. China University of Geosciences, Beijing (in Chinese).

Chen, L. H., Feng, S. W. & Deng, F. F. 2016 Study and application of flood prediction scheme in the upper reaches of Lijiang river basin. *Journal of Guangxi University (Natural Science Edition)* **41** (4), 1298–1305 (in Chinese).

Cheng, G. W. 1988 *Study on Mathematical Model of Deterministic Hydrological Simulation*. Hehai University, Nanjing, China (in Chinese).

Cheng, W. F. 2019 *Study on Runoff Simulation of Wannian Full Watershed Based on HEC-HMS and ELM Model*. Taiyuan University of Technology, Taiyuan, China (in Chinese).

Fang, X. D., Wang, X. Y. & Ou, Y. 2007 The application of SCS method in the calculation of rainfall runoff – taking Miyun Shixia runoff experimental plot as an example. *Journal of Capital Normal University (Natural Science Edition)* **28** (1), 89–92 (in Chinese).

Feng, S. W. 2016 *Research and Application of HEC-HMS and Xin an River Model Flood Prediction*. Guangxi University, Nanning, China (in Chinese).

Ferguson, C. & Fenner, R. 2020 Evaluating the effectiveness of catchment-scale approaches in mitigating urban surface water flooding. *Philosophical Transactions of The Royal Society A: Mathematical, Physical and Engineering Sciences* **378** (2168), 20190203.

Fleury, P., Plagnes, V. & Bakalowicz, M. 2007 Modelling of the functioning of karst aquifers with a reservoir model: application to Fontaine de Vaucluse (South of France). *Journal of Hydrology* **345** (1–2), 38–49.

Ge, H. 2016 *Application and Parameter Calibration of HEC-HMS Model in Semi-Arid and Semi Humid Area*. Hebei University of Engineering, Baoding, China (in Chinese).

Gumindoga, W., Rwasoka, D. T., Nhapi, I. & Dube, T. 2017 Ungauged runoff simulation in Upper Manyame Catchment, Zimbabwe: applications of the HEC-HMS model. *Physics & Chemistry of the Earth Parts A/B/C* **100**, 371–382.

Huang, Y. J. 1995 Summary of the construction and operation of the automatic water condition monitoring and reporting system of Chengbi River reservoir. *Guangxi Water Conservancy and Hydropower* **2**, 14–18 (in Chinese).

Kamali, B., Mousavi, S. J. & Abbaspour, K. C. 2013 Automatic calibration of HEC-HMS using single-objective and multi-objective PSO algorithms. *Hydrological Processes* **27** (26), 4028–4042.

Khaleghi, E., Sadoddin, A., Najafinejad, A. & Bahremand, A. 2020 Flood hydrograph simulation using the SWMM model: a semiarid zone watershed case study, Shiraz Khoshk River, Iran. *Natural Resource Modelling* **33** (2), e12269.

Li, X. C. 2020 Literature review of maskingum method. *Technology Wind* **411** (7), 193–193 (in Chinese).

Li, X. X. & He, H. Q. 2015 *Principle, Method and Application of HEC-HMS Hydrological Modeling System*. China Water Conservancy and Hydropower Press, Beijing (in Chinese).

Liao, F. Q. 2017 Application of hec-hms model in gongcheng river basin. *Hongshui River* **36** (2), 17–20 (in Chinese).

Moriasi, D. N., Arnold, J. G., Liew, M. W. V., Bingner, R. L., Harmel, R. D. & Veith, T. L. 2007 Model evaluation guidelines for systematic quantification of accuracy in watershed simulations. *Transactions of the ASABE* **50** (3), 885–900.

Nikolaidis, N. P., Bouraoui, F. & Bidoglio, G. 2013 Hydrologic and geochemical modeling of a karstic Mediterranean watershed. *Journal of Hydrology* **477** (1), 129–138.

Palanisamy, B. & Workman, S. R. 2014 Hydrologic modeling of flow through sinkholes located in streambeds of cane run stream. *Kentucky. Journal of Hydrologic Engineering* **20** (5), 04014066.

Pan, H. Y. 2014 *Hydrological Model and Application Research of Karst Basin*. China University of Geosciences, Xuzhou, China (in Chinese).

Pan, Z. 2018 *Distributed NAM Hydrological Model Research and System Implementation*. Huazhong University of Science and Technology, Wuhan, China (in Chinese).

Pu, J. B. 2009 *Water Environment Problems in Karst Areas of Southwest China*. The Geographical Society of China, Beijing, China (in Chinese).

Silva, M. M. G. T. D., Weerakoon, S. B. & Herath, S. 2014 Modeling of event and continuous flow hydrographs with HEC-HMS: case study in the Kelani River Basin, Sri Lanka. *Journal of Hydrologic Engineering* **19** (4), 800–806.

Song, X. M., Zhang, J. Y., Zhan, C. S., Wang, X. J. & Liu, C. S. 2015a A review of sensitivity analysis methods of hydrological model parameters. *Advances in Science and Technology of Water Resources* **35** (6), 105–112 (in Chinese).

Song, W. Z., Lei, X. H., Xu, B. L. & Wang, H. 2015b Study on hydrological simulation in Karst Area. *China Rural Water and Hydropower* **7**, 54–57 (in Chinese).

Sun, Y. 2015 *Runoff Characteristics and Flood Forecast of Karst Basin in the Upper Reaches of Qingjiang River*. China University of Geosciences, Wuhan, China (in Chinese).

Sun, L. Q., Hao, Z. C., Wang, J. H., Nistor, I. & Seidou, O. 2014 TMPA evaluation and correction of satellite precipitation data. *Journal of Water Conservancy* **45** (10), 1135–1146 (in Chinese).

Suo, L. T., Wan, J. W. & Lu, X. W. 2007 Improvement and application of TOPMODEL model in Karst Area. *Carsologica Sinica* **1**, 67–70 (in Chinese).

US Army Corps of Engineers 1994 *Engineering and Design: Flood-Runoff Analysis (Engineer Manual 1994 1110-2-1417)*. US Army Corps of Engineers, Washington, DC, USA.

Wang, J. T. 2018a *Early Warning Simulation and Research of Mountain Torrents in Typical Small Watershed of North China Based on HEC-HMS Model*. University of Jinan, Jinan, China (in Chinese).

Wang, Q. W. 2018b *Study on the Impact of Climate Change on the Runoff From the Bileu River Basin*. Taiyuan University of Technology, Taiyuan, China (in Chinese).

Wang, Y., Sang, G., Jiao, C., Xu, Y. & Zheng, H. 2018 Flood simulation and parameter calibration of small watershed in hilly area based on HEC-HMS model. *IOP Conference Series: Earth and Environmental Science* **170**, 032093.

Wang, J., Song, X. M., Zhang, J. Y., Wang, G. Q. & Liu, J. 2019 Comparative study on flood model simulation of small and medium-sized basins. *China Rural Water Conservancy and Hydropower* **441** (7), 76–80 (in Chinese).

Xu, B. L., Dong, Z. C. & Hong, X. 2017 Construction and application of aggregate karst hydrological model. *Water Conservation* **33** (2), 37–42 (in Chinese).

Zettel, V. & Hitzmann, B. 2017 Optimization of the production parameters for bread rolls with the Nelder–Mead simplex method. *Food & Bioproducts Processing* **103**, 10–17.

Zhang, C., Jiang, Y. J., Lian, Y. Q., Pei, J. G., Jiang, G. H. & Wang, J. L. 2007 Using SWMM model to simulate the rainfall runoff process of karst peak cluster depression system. *Hydrogeology Engineering Geology* **34** (3), 10–14 (in Chinese).

Zhang, Z. C., Yan, D. D. & Zhong, J. M. 2017 The induction of calculation method of surface runoff with super permeability. *Engineering and Technological Research* **8**, 79–80 (in Chinese).

Zhang, S., Wang, J. & Xu, Z. 2019 The application of HEC-HMS in mountain torrents simulation of northern small watershed. *IOP Conference Series Earth and Environmental Science* **252**, 052060.

Zhao, R. H., Zhao, H. Q., Wang, X. J., Zhao, Y. & Zhang, L. Z. 2018 Application of the HEC-HMS model for flood simulation in ungauged mountainous area. *DEStech Transactions on Environment, Energy and Earth Sciences* **6**, 203–208.

Zhao, Y., Liao, W. & Lei, X. 2019 Hydrological simulation for karst mountain areas: a case study of central Guizhou Province. *Water* **11** (5), 991.

First received 10 May 2020; accepted in revised form 29 October 2020. Available online 9 December 2020